

Accelerating Large-Scale Linear Algebra Using Variational Quantum Imaginary Time Evolution

Willie Aboumrad*, Daiwei Zhu*, Claudio Grotto*, François-Henry Rouet†, Jezer Jojo†, Robert Lucas†, Jay Pathak†, Ananth Kaushik*, Martin Roetteler*

*IonQ Inc., 4505 Campus Dr, College Park, MD 20740, USA

†Ansys, Inc., 2600 Ansys Drive, Canonsburg PA 15317, USA

Abstract—Graph partitioning techniques enhance the efficiency of solving large-scale linear systems in the context of Finite Element Analysis (FEA). Even for systems of linear equations that are highly sparse, their direct solution via factorization methods, such as LU or Cholesky decomposition, is computationally expensive due to the introduction of non-zero elements, or “fill-in.” We introduce a quantum approach to the graph partitioning problem based on the variational quantum imaginary time evolution algorithm (VarQITE), allowing to solve the combinatorial optimization problem of reordering of sparse matrices to minimize the fill-in. We develop a hybrid quantum/classical pipeline to accelerate Finite Element solvers by integrating the VarQITE algorithm into the production workflow of Ansys’ industrial software LS-DYNA. This allows to study multiple different types of FEA problems, ranging from mechanical engineering to computational fluid dynamics.

We prove out that VarQITE positively impacts LS-DYNA workflows by measuring the wall-clock time to solution of FEA problems when compared against the classical heuristic graph partitioning solver in LS-DYNA. The selected instances cover a range of FEA problems, including simulation of blood pumps, roof crushing of cars, and vibration analysis of cars. We report performance results for our hybrid quantum-accelerated workflow on FEA meshes of up to 5.9M vertices and 55 million edges. We find that the wall clock time of the heuristics solutions used in the industry-grade solver is improved by up to 12%. We also execute the VarQITE algorithm on quantum hardware (IonQ Aria and IonQ Forte) and find that the results are comparable to noiseless and noisy simulations. Finally, we introduce a hybrid technique for post-processing the found solutions with classical refinement heuristics such as Fiduccia-Mattheyses.

Our results highlight the impact of quantum computing on large-scale FEA problems. Our results are evidence of potential commercial quantum value within the NISQ era.

Keywords—Quantum computing, Quantum imaginary time evolution, Finite Element Methods, Finite Elements Analysis.

I. INTRODUCTION

Solving a linear system $Ax = b$, with A and b known, is the main computational bottleneck in a number of scientific and commercial computing applications. The matrix A typically is large and *sparse*, with representative cases having tens to hundreds of millions of rows and columns, yet only a small number of entries per row are non-zero. Such matrices are typically distributed across multiple compute nodes, and only the non-zero entries are stored. These linear systems cannot be solved directly using Gaussian elimination due to large cost. Instead, a variant is used that factors the matrix into upper and lower triangular matrices, allowing the linear system

to be easily solved with forward elimination and backward substitution.

The factorization step eliminates non-zero entries in the lower triangle of the matrix by subtracting previous rows. Zeroing out one entry often introduces new non-zero entries, a process called fill-in. Fill-in dynamically increases the computational burden of the factorization step.

The diagram in Figure 1 illustrates how permuting the rows and columns of an “arrowhead” matrix can dramatically reduce the fill-in. In practice, finding an optimal reordering of a sparse matrix that minimizes fill-in is a combinatorial optimization problem, i.e., an NP-Complete problem [1]. Finding permutations to reduce fill-in is difficult, especially when matrices are distributed over thousands of processors. As the processor count increases, the reordering step can dominate the entire run-time of a Finite Element Analysis (FEA) application.

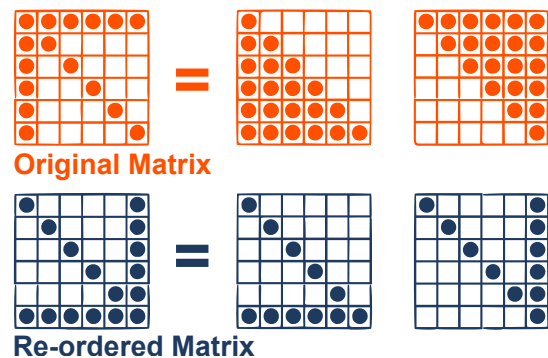


Fig. 1: Reordering the rows of a matrix to minimize the fill-in for Gaussian elimination. The matrix on the left undergoes LDL^T decomposition which introduces extra non-zero elements (“fill-in”). The goal of reordering the original matrix is to minimize this “fill-in” which reduces the number of operations required to solve the linear system.

The reordering problem is well-studied and many classical heuristics are available. In computational mechanics, “Nested Dissection,” a divide-and-conquer approach introduced in 1973 [2], remains the most successful. In this method, the sparse matrix is represented as an undirected graph in which the vertices represent rows and columns of the matrix and the edges represent the non-zero entries. This graph is recursively partitioned into subgraphs using *separators*, small subsets of vertices whose removal allows the graph to be partitioned

into disjoint subgraphs with at most a constant fraction of the number of vertices. Most implementations of Nested Dissection, such as METIS [3] and variants thereof, rely on a so-called *multilevel* scheme, where the graph to be partitioned is first *coarsened* into a smaller graph. The coarse graph is partitioned into two parts, and the partition is then *projected* onto the original graph and transformed into a vertex separator before being refined. The bipartition of the coarse graph is a critical component and the focus of our study.

The Graph Partitioning Problem (GPP) has a long history in theoretical computer science, and countless applications in scientific computing, task scheduling, social networks, VLSI design, etc. The GPP seeks to partition the vertices of a graph into balanced parts, while minimizing an objective function such as the number of cut edges. It is known that no polynomial time algorithm can obtain balanced graph partitions within a finite approximation factor [4]. A range of heuristic algorithms have been developed that can efficiently produce solutions in practical settings. In this work we explore the potential of quantum algorithms to obtain higher quality graph partitions, exploiting quantum resources to improve upon leading classical heuristics. In particular, we adapt a variational quantum imaginary time evolution (VarQITE) algorithm [5] for approximately solving multiple GPPs constructed by Ansys' LS-DYNA [6] commercial multiphysics simulation software. Concretely, we demonstrate the applicability of our novel hybrid quantum-classical by integrating quantum computations executed on IonQ's Aria and Forte into a large-scale Implicit Mechanics simulation conducted by LS-DYNA, and discuss encouraging results highlighting early evidence of quantum utility in the NISQ era.

The rest of this paper is organized as follows. In Section II, we describe the GPP in some detail, along with its formulation as a Hamiltonian Energy Minimization problem. In addition, we briefly describe the VarQITE algorithm. In Section III we explain the structure and formulation of our quantum ansatz as well as how to apply VarQITE to obtain high-quality approximations of the GPP. We also describe the pipeline of integration of VarQITE into LS-DYNA and the metrics for evaluation and comparison of solutions to the classical heuristic graph partitioning solver in LS-DYNA. In Section IV we discuss the results of our quantum computations both from noiseless simulations as well as from executions on IonQ quantum hardware Aria and Forte. Finally, in Section V we discuss ongoing research and lay out an optimistic outlook for the future development of our quantum-classical methods.

II. PROBLEM FORMULATION

A. The Graph Partitioning Problem (GPP) as a Quadratic Program (QP)

Given a (vertex- and edge-) weighted graph $G = (V, E)$, a k -way partition of the graph is a family of disjoint subsets V_1, V_2, \dots, V_k of V s.t. $V_1 \sqcup V_2 \dots \sqcup V_k = V$. When $k = 2$, this is referred to as a *bipartition*. Different Graph Partitioning Problems (GPP) can be formulated based on the objective function to minimize and constraints placed on the partition.

A typical objective function is to minimize the sum of the weight of *cut edges*, edges which connect vertices belonging to different parts, i.e., to the set $\{(v_i, v_j) \in E \text{ with } v_i \in V_i, v_j \in V_j, i \neq j\}$. A typical constraint is to enforce that parts have equal or similar sizes. In the context of multilevel Nested Dissection, there is freedom in the choice of the constraints. Our choice is to find a bipartition $\{V_1, V_2\}$ such that $|V_1|$ and $|V_2|$ do not exceed $(\frac{1}{2} + \nu)|V|$ where $|\cdot|$ denotes the sum of vertex weights. In this paper, we set $\nu = 0.05$.

In symbols, we formulate our GPP as the following QP:

$$\begin{aligned} \text{minimize}_x \quad & \sum_{(i,j) \in E} w_{ij}(x_i + x_j - 2x_i x_j), \\ \text{s.t.} \quad & \sum_i v_i x_i \leq (1/2 + \nu)\Omega \\ & \sum_i v_i (1 - x_i) \leq (1/2 + \nu)\Omega \\ & x_i \in \{0, 1\}. \end{aligned} \quad (1)$$

Here, the w_{ij} denote the edge weights, the v_i denote the node weights, Ω denotes the total sum of the node weights, and the Boolean variable x_i determines whether the i th node belongs to V_1 ($x_i = 0$) or V_2 ($x_i = 1$).

B. GPP as a Quadratic Unconstrained Binary Optimization (QUBO) problem

In order to leverage quantum resources for solving our GPP, we first formulate the QP in equation (1) as a QUBO. Standard techniques convert inequality constraints into penalty terms by introducing slack variables. This translates into higher qubit requirements when minimizing on quantum hardware. We opt for the following penalty instead:

$$P(x) = \left(\sum_i v_i x_i - \sum_i \frac{v_i}{2} \right)^2. \quad (2)$$

This quadratic term penalizes deviations in the total node weight on each side of the partition; it is minimized when the sum of the node weights in the two partitions are equal.

Thus, the problem at hand is to minimize the unconstrained objective

$$C(x) = \sum_{(i,j) \in E} w_{ij}(x_i + x_j - 2x_i x_j) + \lambda P(x). \quad (3)$$

Here $\lambda > 0$ is a tunable hyper-parameter that defines a trade-off between lower weight and more balanced cuts.

C. From GPP to Hamiltonian Energy Minimization

Given $C(x)$, we encode our GPP as a Hamiltonian Energy Minimization problem by constructing a Hamiltonian H_C on $n = |V|$ qubits such that

$$H_C |x\rangle = C(x) |x\rangle,$$

using standard techniques. In particular, we obtain H_C by replacing each x_j in the expression of $C(x)$ by the operator

$$\hat{X}_j = \frac{1}{2}(I - Z_j),$$

where I denotes the identity operator on n qubits and Z_j denotes the Pauli-Z operator acting on the j th qubit. Notice that \hat{X}_j is diagonal with respect to the computational basis, and its eigenvalues are zero and one; in particular,

$$\hat{X}_j |x\rangle = x_j |x\rangle.$$

D. Variational Quantum Imaginary Time Evolution

Quantum imaginary time evolution is a powerful approach to compute the ground state of physical system. It expresses the ground-state as the long-time limit of the imaginary time Schrödinger equation. The variational imaginary time evolution (VarQITE) algorithm is designed to efficiently prepare the ground state of a Hamiltonian, which encodes a combinatorial optimization problem (though it is not limited to this class of problems). Imaginary time evolution, a concept originating in quantum many-body physics, systematically projects a given initial state $|\Psi(0)\rangle$ onto the ground state of H_c by evolving it in imaginary time $\tau = it$, where t is the real time parameter. This process is governed by the imaginary-time Schrödinger equation

$$\frac{\partial}{\partial \tau} |\Psi(\tau)\rangle = -(H_c - E_\tau) |\Psi(\tau)\rangle, \quad (4)$$

where $E_\tau = \langle \Psi(\tau) | H | \Psi(\tau) \rangle$ is the instantaneous energy resulting from enforcing normalization. For a time-independent Hamiltonian H_c , the solution is given by

$$|\Psi(\tau)\rangle = \frac{e^{-\tau H_c}}{\sqrt{\langle \Psi(0) | e^{-2\tau H_c} | \Psi(0) \rangle}} |\Psi(0)\rangle. \quad (5)$$

As $\tau \rightarrow \infty$, and assuming that $|\Psi(0)\rangle$ has a non-zero overlap with the ground state $|\Psi_{GS}\rangle$, this evolution exponentially suppresses excited-state components, thus converging to $|\Psi_{GS}\rangle$.

Since directly implementing the operator $\exp(-H_c \tau)$ on a quantum computer is challenging, we can instead approximate imaginary time evolution variationally. We introduce a parameterized ansatz $|\Psi(\theta)\rangle$ with parameters that change as a function of iteration number. The goal is to adjust these parameters $\theta(\tau)$ such that the state $|\Psi(\theta(\tau))\rangle$ closely approximates the true imaginary-time evolved state $|\Psi(\tau)\rangle$.

To achieve this, a common approach is to apply the McLachlan variational principle to project the imaginary time evolution onto the variational manifold defined by $|\Psi(\theta)\rangle$ [7], [8], which would require $\mathcal{O}(m^2)$ circuit evaluations per time step, where m is the number of terms in a Pauli-decomposition of H_c . Instead, we adopt the approach presented in [9], which enforces the imaginary time evolution of each Pauli term P_α in H_c by

$$\begin{aligned} \frac{\partial \langle P_\alpha \rangle}{\partial \tau} &= \sum_j 2 \operatorname{Re} \left[\langle \Psi(\theta) | P_\alpha \frac{\partial}{\partial \theta_j} | \Psi(\theta) \rangle \right] \dot{\theta}_j \\ &= -\langle \Psi(\theta) | \{P_\alpha, H_c - E_\tau\} | \Psi(\theta) \rangle, \end{aligned} \quad (6)$$

with $\dot{\theta}_j = \partial \theta_j / \partial \tau$. Applying this condition to all P_α terms in the Hamiltonian H_c yields the linear system

$$G \cdot \dot{\theta} = D, \quad (7)$$

where

$$G_{\alpha,j} = \operatorname{Re} \left[\langle \Psi(\theta) | P_\alpha \frac{\partial}{\partial \theta_j} | \Psi(\theta) \rangle \right], \quad (8)$$

$$D_\alpha = -\frac{1}{2} \langle \Psi(\theta) | \{P_\alpha, H_c - E_\tau\} | \Psi(\theta) \rangle. \quad (9)$$

Using the parameter-shift rule [10], [11], each column of G can be determined from just two circuit evaluations. Moreover, if the Hamiltonian H_c consists solely of Pauli-Z operators (as those in QUBO formulations), all P_α terms commute, allowing the calculation of D from a single circuit evaluation. Thus, at each time step, the parameters θ can be updated using a forward Euler method, $\theta \rightarrow \theta + \Delta\tau \dot{\theta}$, where $\dot{\theta}$ is obtained by inverting equation (7). This procedure requires only $2m + 1$ circuit evaluations per time step, offering a substantial improvement in efficiency compared to previous VarQITE approaches [7], [8].

III. METHODS

A. Application of VarQITE to the Graph Partitioning Problem

VarQITE can be used to solve the GPP arising in a variety of engineering FEM applications. We focus on three specific problem instances of practical interest, detailed in Table I. Each problem has graphs with millions of edges and needs to be coarsened down to manageable sizes to be analyzed by the quantum algorithm. The LS-DYNA workflow developed by Ansys is used to perform the graph coarsening and reconstruction after the graph partitioning, as visualized in Figure 2.

TABLE I: Summary of the problem instances analyzed in this paper. Vertices and edges are expressed in millions(M). The roof crush simulation was performed with respect to a publicly available FEA mesh of a Toyota Yaris, the vibration analysis was performed with respect to a Honda Accord model.

	BloodPump	RoofCrush	VibrationAnalysis
Number of vertices	0.2M	0.6M	5.9M
Number of edges	3.5M	5M	55M
Mesh type	Tets, 2.5D	Shells, 2.5D	Tets, 2.5D
Origin	Ansys, FDA	NCAC	NHTSA, Arup

The LS-DYNA tool uses nested dissection to reduce the matrix representation of the mesh (which is represented as a graph via its adjacency matrix) to smaller chunks. The total number of levels of nested dissection performed by an external partitioner can be set as a parameter in the LS-DYNA control card. The tool then performs a graph coarsening to reduce the size of the graph. The degree of coarsening required (number of vertices of the coarse graph) may also be set as a parameter for the tool. The coarse graph has vertices and edges with large vertex and edge weights due to the high degree of coarsening required so that the problem can fit on current quantum computers, i.e., graphs with 10s of vertices. The size of the

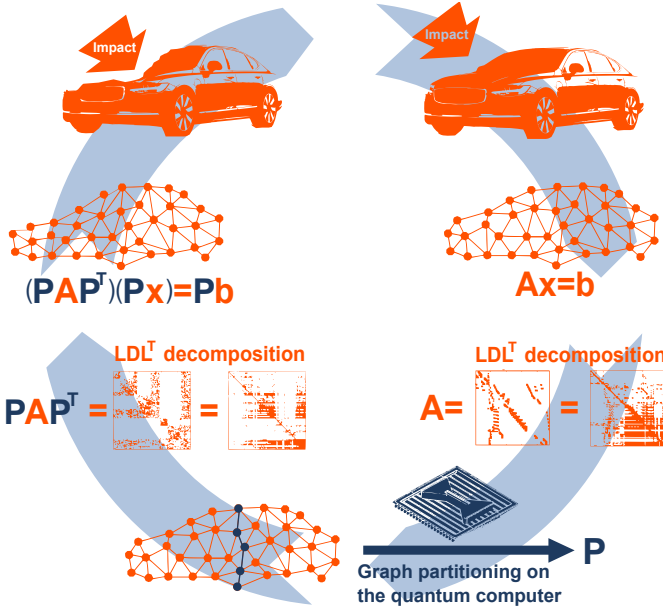


Fig. 2: The execution flow chart of LS-DYNA including calls to the quantum computer. Starting from the upper right is a car which is modeled with a finite element mesh, together with an impact. The time evolution is given as a linear system of equations to be solved $Ax = b$. Here A is a sparse matrix which when decomposed using LDL^T decomposition leads to the dense matrices shown in the figure. A graph partitioning problem is formulated from the adjacency graph of A and is solved on the quantum computer, indicated by an ion trap on the lower right. This yields P , a permutation matrix to reorder A obtained by solving the graph partitioning problem recursively. The solution is used to partition the mesh as illustrated by the blue line of vertices. The reordered matrix A retains a sparse structure after LDL^T decomposition. The linear system is now solved using the the reordered matrix A and the reordered vector b to obtain the required deformation simulation of the original model. The process can be iterated.

coarse graph will increase with scaling the quantum hardware to larger numbers of qubits. The graph partitioning problem is now formulated to find the best bi-partition of the graph with the least edge cut cost while maintaining nodal weight balance between the two subgraphs (within 5% nodal weight balance). This graph partitioning optimization problem is performed on the quantum simulator/QPU hardware using VarQITE which produces a distribution of solution bitstrings to the problem. The bitstrings are the separators required to the partition the coarse graph into two subgraphs. If there is more than one level of nested dissection, the same procedure is repeated on the two subgraphs produced after the first level of nested dissection. The two subgraphs are once again coarsened and the graph partitioning is performed to produce more subgraphs. After the required number of levels of nested dissection are completed, the original matrix is reordered using the set of smaller graphs that have been produced by the partitioning.

This reordered matrix has hopefully, a better “fill” thereby reducing the number of non-zeros (memory requirement to store the matrix) and the number of computations required to perform the linear system solve for the FEM simulation.

In Section IV-A we compute the resources required to solve the linear system by computing the number of non-zero fills arising from the LDL^T decomposition of the reordered matrix and the number of linear algebra computations required using symbolic factorization. The execution of the LS-DYNA tool is terminated after this computation and the number of non-zeros and number of operations are used a factor of merit to assess the quality of the separators produced by the VarQITE optimization when compared with the internal classical heuristic LS-Gpart provided within LS-DYNA. In Section IV-C, we also compare the total wall clock time for the linear system solve using the VarQITE separators and the LS-GPart separators. In this case, we analyze the RoofCrush problem, the BloodPump problem, and the VibrationAnalysis problem. For each, we compute the total time for symbolic factorization, the actual factorization of the matrix and the time to solve the linear system.

B. Optimizing the VarQITE ansatz

As described in Section II-D, the VarQITE algorithm uses a parametrized quantum wavefunction to approximate the true wavefunction. The parametrized wavefunction can be instantiated using a quantum circuit ansatz consisting of parametrized quantum gates (1-qubit and 2-qubit quantum gates whose rotation angles are the parameters of the wavefunction). Exactly which gates are chosen and how they are ordered in the ansatz has a great impact on the convergence behavior of the VarQITE algorithm indicating that ansatz design is critical.

We introduce the HeavyNeighborsAnsatz, a configurable layered ansatz that entangles certain qubits by exploiting the graph structure. In this ansatz, every vertex of the graph is represented by a qubit and every entangling 2-qubit gate is represented by a $R_{ZY}(\theta)$ gate with a parametrized angle θ . Given a graph G , a number of layers ℓ , and an ℓ -vector \mathbf{g} determining the desired number of gates per layer, we construct the corresponding HeavyNeighborsAnsatz one layer at a time, as follows. At layer 0, we sort the edges in the graph and append parametrized two-qubit gates on the pairs of qubits corresponding to the \mathbf{g}_ℓ heaviest edges. At layer $k < \ell$, we sort the nodes in G according to the total edge weight of their corresponding radius (k) ego graph. Recall that the radius r ego graph of a node $v \in G$ is the induced subgraph centered at v and including all nodes within a distance r of v . Then we place parametrized two-qubit gates on the qubits corresponding to the nodes with the heaviest neighborhoods; in particular, if $s^{(k)}$ denotes the indices of the nodes in G sorted by decreasing radius (k) ego graph weight, we place entangling gates on qubits $(s_1^{(k)}, s_2^{(k)}), (s_1^{(k)}, s_3^{(k)}), \dots, (s_1^{(k)}, s_{\mathbf{g}_k}^{(k)})$.

Fig 3 shows an example of a 5 qubit parametrized ansatz. The VarQITE algorithm variationally optimizes the parameters of this ansatz to obtain the solutions to the graph partitioning problem. From a network flow perspective, the

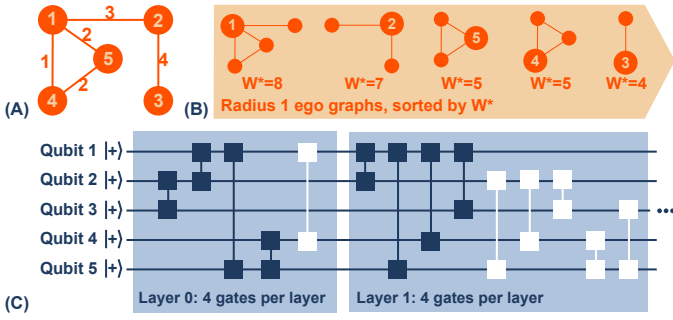


Fig. 3: VarQITE ansatz: (A) An example of a 5 node graph with the nodes and edge weights labeled, (B) The nodes sorted according to W^* , the total edge weight of their induced ego graph of radius 1. (C) The VarQITE ansatz generated using the ego graphs. In this illustration, the ansatz is constructed with 4 gates per layer (this number can be adjusted as required). The included gates are shown in dark blue while the excluded gates are shown in white (since there are only 4 gates per layer, some of the gates will need to be excluded). The first layer (Layer 0) has entangling gates between qubits connected by the graph edges in the descending order of edge weights. The second layer (Layer 1) has entangling gates between qubits sorted by their induced ego graph of radius 1. More layers may be added, generated by ego graphs of radii equal to 2, 3, 4, etc.

HeavyNeighborsAnsatz entangles qubits that correspond to nodes serving as gateways to regions where the accessible flow is large. These nodes have the highest impact on the cut size of a partition because they span the heaviest edges in the graph. The parametrized entangling gate across each such pair allows the ansatz to decide whether to increase the probability of observing one of the inputs in the opposite side of the partition.

In addition, the layered construction of the ansatz allows each candidate partition, encoded as a computational basis state in the superposition supported by the parametrized trial state, to be iteratively refined through a sequence of entangling gates as it goes through the layers. This is akin to the leading local classical heuristics detailed in Section III-D. The refinement process is evident in the HeavyNeighborsAnsatz, as each layer incorporates increasingly global information. The first layer features the most “local” connectivity information based on direct connections between nodes, i.e. the edges in the graph. In contrast, the final layer places gates using ego graphs with the largest radius.

For the noiseless simulations described in Section IV-A, we used a 2-layer HeavyNeighborsAnsatz, with layer 1 consisting of all gates generated from the induced ego graph of radius 1. Only gates that were already included in layer 0 were excluded in layer 1. This approach was chosen to enhance the expressibility of the ansatz and establish the baseline performance of the VarQITE algorithm. However, this technique requires a substantial number of two-qubit gates that makes it impractical for noisy NISQ-era QPU. Specifically, for a graph with n nodes, the full ansatz would use $n(n-1)/2$

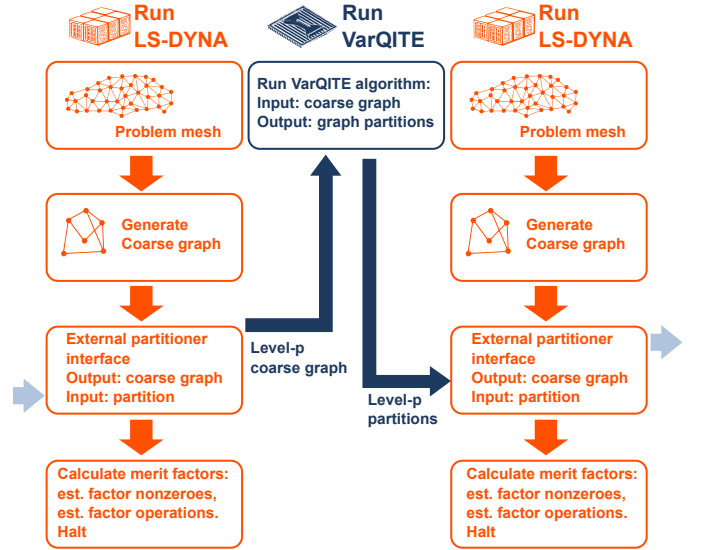


Fig. 4: Integration of VarQITE into LS-DYNA for the evaluation of the factor of merit in a level-1 nested dissection process. LS-DYNA (orange arrows and boxes) executes two times in this integration framework. The VarQITE algorithm (blue arrows and boxes), which computes optimal partitions, operates externally between the two executions of LS-DYNA.

two-qubit gates, requiring the execution of n^2-n+1 circuits on n qubits, each with $n(n-1)/2$ two-qubit gates, at each VarQITE iteration to compute the expectation value of the hamiltonian and its gradients. Consequently, for the hardware runs described in Section IV-D, we used an optimized ansatz in which we truncated the HeavyNeighborsAnsatz, leading to a variant with a restricted number of gates per layer to reduce the total number of gates in the ansatz.

C. Evaluation of the merit factors

To assess the value of the VarQITE algorithm’s solution, it is essential to incorporate it into the LS-DYNA workflow. We developed a modified LS-DYNA version that enables an external subroutine call for graph partitioning, as shown in the red blocks of Fig. 4. Through three separate runs, LS-DYNA first extracts the coarsened graph, then the VarQITE algorithm partitions it, and finally, LS-DYNA calculates the merit factors of the given partition. This process allows for a direct performance comparison between LS-DYNA’s internal classical heuristic and the external VarQITE algorithm, as detailed in Section III-A.

The VarQITE algorithm’s strength lies in its ability to generate a sampled distribution of solutions that is focused on a collection of low objective function values. This collection potentially includes the optimal solution to the Graph Partitioning Problem (GPP), and importantly, allows for the exploration of merit factors from multiple near-optimal solutions, rather than being limited to a single value. These multiple near-optimal solutions are fed back into the LS-DYNA workflow via the external partitioner interface. LS-DYNA then partitions the

graph and calculates the relevant merit factors before stopping execution.

As shown in Figure 4, the procedure used to evaluate the partition for a single-level (level-1) nested dissection involves running LS-DYNA until the coarse graph is generated, at which point the program halts and the coarse graph is extracted. The VarQITE algorithm then solves the GPP on the extracted coarse graph. When the VarQITE algorithm converges, the quantum circuit is measured many times (shots) to obtain a sampled distribution of solutions from the underlying probability distribution of the quantum wavefunction. Notably, this sampled distribution contains multiple near-optimal solutions to the GPP, and is focused on low objective function values which may include the optimal solution.

This integrated process extends to multiple levels of nested dissection. To evaluate level- L nested dissection, LS-DYNA is executed a total of $L + 1$ times. On the l -th level of nested dissection, the VarQITE algorithm is executed to compute partitions for the 2^{l-1} coarse graphs extracted from the (l) -th level of nested dissection. These computed partitions are then returned to LS-DYNA by the external partitioner to compute the $(l + 1)$ -th level coarse graphs and so on till all L levels of nested dissection are completed and the final merit factors are obtained.

D. Enhancing VarQITE algorithm with classical heuristic refinement

The graph partitioning problem has been studied extensively over the years and numerous classical heuristics have been developed to solve this problem. Notable examples include the Kernighan-Lin (KL) algorithm [12], the Fiduccia-Mattheyses (FM) algorithm [13], and more recently, reinforcement learning-based approaches [14]. These methods are widely applied in Finite Element Analysis, VLSI design, parallel computing and other optimization tasks. We propose an approach to enhance the performance of the VarQITE algorithm executed on noisy quantum hardware by incorporating a modified version of the Fiduccia-Mattheyses algorithm.

Given a graph $G(V, E)$, the original FM algorithm seeks partitions with near-minimal edge cut through a local search strategy based on the Gain function $D[v]$, which can be computed efficiently:

$$D[v] = \sum_{u \in N(v)} w(v, u) \cdot (-1)^{\text{same_partition}(u, v)} \quad (10)$$

Here, $N(v)$ is the set of neighbors of vertex v , $w(v, u)$ is the edge weight of the edge connecting vertices (u, v) , and $\text{same_partition}(u, v)$ is a Boolean function indicating whether the two vertices belong to the same graph partition.

In its standard form, the FM algorithm initializes a partition with equal cardinality and improves it through an iterative swapping process. At each step, a node is selected from one partition based on the largest $D[v]$ value and moved to the other partition. The algorithm alternates between partitions ensuring an equal number of moves from both sides. This process continues for a maximum of M iterations or until

no further improvement is observed. While this alternating strategy maintains cardinality balance, it is unsuitable for applications where nodal weight balance is a constraint.

To address this limitation, we introduce a key modification to the FM algorithm. At each step, the algorithm identifies the partition with the greater nodal weight $P[b]$, where b represents the weight difference between P_0 and P_1

$$P[b] = \begin{cases} P_0, & b \geq 0, \\ P_1, & b < 0. \end{cases} \quad (11)$$

Instead of alternating between partitions, nodes are always removed from the partition with the greater total nodal weight. This modification ensures that every move contributes to reducing both edge cut and nodal-weight imbalance, rather than simply maintaining equal cardinality. However, even with modifications, the FM algorithm can struggle to converge when handling multiple objectives or when constraints are reformulated as optimization objectives [15]. A well-chosen initialization can mitigate these difficulties, naturally motivating the integration of the FM algorithm with the VarQITE algorithm where the distribution of solutions provided by VarQITE can be chosen as the initial point for the modified FM algorithm.

The modified FM algorithm is detailed in Algorithm 1 and serves as an efficient post-processing step to refine the ensemble of partitions generated by VarQITE. Its local search mechanism complements the global optimization of VarQITE by efficiently exploiting high-quality regions in the solution space. This hybrid quantum-classical approach accelerates convergence toward near-optimal solutions, enhancing both the utility of the quantum algorithm and overall computational efficiency. Additionally, it acts as an effective error mitigation strategy in the NISQ era, improving the reliability of results from noisy quantum hardware. More detailed information about the refinement is provided in the Supplementary Information Section VI-A.

IV. RESULTS

In this section, we first present the results from running VarQITE on a noiseless statevector simulator using the ansatz described in Section III-B. This is followed by a comparison of the merit factors obtained from the GPP solutions produced by VarQITE and the classical heuristic in LS-DYNA. We then present the results from executing VarQITE on IonQ quantum hardware and the refinement of the GPP solutions using the modified FM algorithm.

A. Results of noiseless VarQITE simulations

The two GPP problems of interest - RoofCrush and BloodPump were executed using VarQITE on a noiseless quantum simulator. The VarQITE optimization requires $2n$ gradient calculations of the quantum ansatz corresponding to n parameters at each iteration. For each circuit execution, 1,000 shots were used to sample the quantum state. We explored graph coarsening of the two problems from 10 to 32 vertices, with

Algorithm 1 Modified Fiduccia-Mattheyses Algorithm

Require: Graph $G(V, E)$, max iterations M , nodal weight imbalance tolerance ϵ

Ensure: Partition bitstring \mathbf{p}

- 1: Initialize random bitstring \mathbf{p} , with length $n \leftarrow |V|$ and equal cardinality
 - 2: Compute initial nodal weight balance b
 - 3: **for** $iteration = 1$ **to** M **do**
 - 4: Compute $D[v]$ for each node v
 - 5: Mark all nodes as "untouched"
 - 6: Set edge-cut gain $g \leftarrow 0$
 - 7: **for** $step = 1$ **to** n **do**
 - 8: $v^* \leftarrow \arg \max_{v \in P[b], v \notin \text{touched}} D[v]$
 - 9: **if** no valid v^* found **then**
 - 10: **break**
 - 11: **end if**
 - 12: Swap v^* to the opposite partition
 - 13: Mark v^* as "touched"
 - 14: Update edge-cut gain $g \leftarrow g + D[v^*]$
 - 15: Update weight balance b
 - 16: Update $D[v]$ for affected nodes
 - 17: **end for**
 - 18: $g^* \leftarrow$ largest g in the current $iteration$ with $b \leq \epsilon$
 - 19: **if** $g^* \leq 0$ **then**
 - 20: **break**
 - 21: **end if**
 - 22: Revert \mathbf{p} to the configuration that achieved g^*
 - 23: **end for**
 - 24: **return** Final partition bitstring \mathbf{p}
-

each vertex mapped on to one qubit of the quantum circuit. We studied the performance of the VarQITE algorithm with one and two levels of nested dissection, denoted respectively Level-1 or L1, and Level-2 or L2. All simulations were run using the IonQ statevector simulator. Simulations for graphs with 24 or fewer nodes were executed in parallel on AMD EPYC 7763 compute nodes, while simulations for graphs with more than 24 nodes were executed on Nvidia A100 GPUs.

We define the Approximation Ratio as the energy of the solution divided by the energy of the optimal solution, where the energy of a solution is obtained by evaluating the QUBO hamiltonian defined in Section II-C on the solution. The value of 1-AR should decrease as the VarQITE algorithm evolves, because the AR of the solutions found would improve towards to optimal solution. A value of 0.0 on the y-axis is reached when the optimal solution is sampled.

Figure 5 shows the convergence behavior of the VarQITE algorithm for the RoofCrush and the BloodPump GPP problems. The y-axis represents the value of 1 minus the Approximation Ratio (AR) of the solutions found at a given iteration of VarQITE. At each iteration the measurement of the quantum circuit produces 1,000 binary bitstrings, which represent potential partitions. The best solution sampled at any given iteration is shown in orange. The average value over

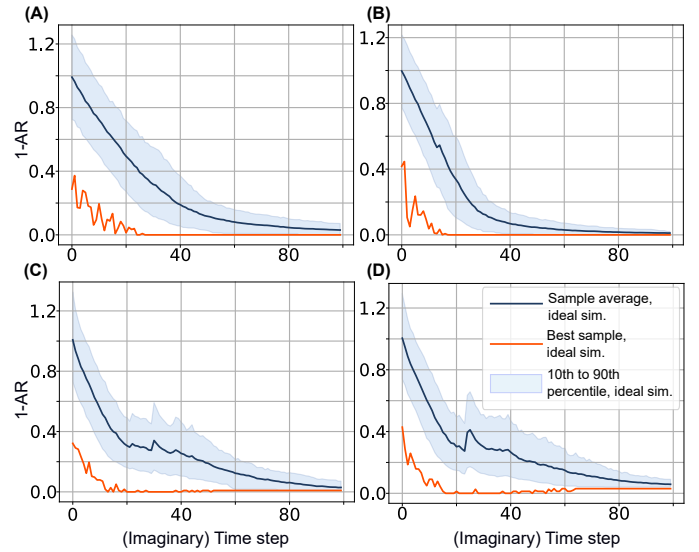


Fig. 5: Convergence of VarQITE on a Noiseless Simulator: Plots for (A) RoofCrush 30 nodes, (B) RoofCrush 32 nodes, (C) BloodPump 30 nodes, (D) BloodPump 32 nodes. The y-axis shows the value of 1-AR where AR is the Approximation Ratio of the solution. The solid blue and purple lines correspond to the average and best value from the sampled distribution, respectively. The shaded blue region corresponds to the values between the 10th and 90th percentile of the sampled distribution. All results were obtained using 2,000 shots to sample the quantum circuit.

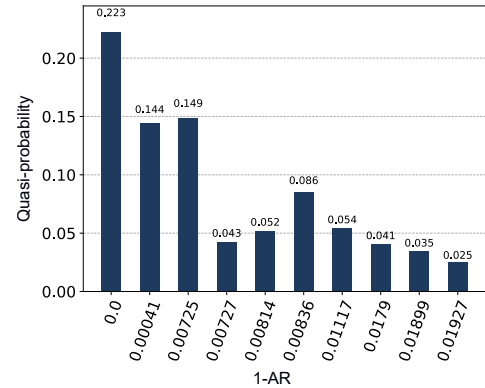


Fig. 6: Probability histogram of a few unique solutions with the lowest objective function values from RoofCrush GPP problem, coarsened to 32 nodes. The x-axis shows solutions with increasing values of 1 minus the Approximation Ratio (AR). The optimal solution to the GPP problem is the first bar from the left, where the 1-AR value is 0.0.

the entire sampled distribution is depicted in dark blue, while the lighter blue band indicates the range of values between the 10th and 90th percentiles of sampled distribution. As the VarQITE algorithm iteratively amplifies the probability of states with lower energy, the initial distribution of solutions (which is broad and uniform) rapidly narrows, as shown by the gap between the 10th and 90th percentiles becoming

increasingly smaller over successive iterations. Ultimately, the distribution peaks over the optimal solution and other near-optimal solutions. This convergence behavior is observed consistently in the plots presented and the optimal solution is found in each case.

Figure 6 shows the sampled distribution from the last iteration of the VarQITE algorithm for RoofCrush GPP problem with 32 nodes. The first bar from the left represents the optimal solution to the problem with a 1-AR value of 0.0. This solution is also sampled with a high probability of $\sim 26\%$ with various other near-optimal solutions sampled with decreasing probabilities. This shows that the VarQITE algorithm has succeeded in converging to a distribution peaked over the optimal and near-optimal solutions.

B. Comparing merit factors between VarQITE and LS-GPart

The estimated number of non-zeroes in the triangular factor and the estimated number of operations required to factor the stiffness matrix during the symbolic factorization step were the figures of merit used in this analysis. These metrics, which are influenced by the provided partition, are crucial parameters affecting the total time to solution of FEA problem. In this section, we compare the merit factors produced by using the VarQITE partitioner against the LS-DYNA internal heuristic (LS-GPart). The VarQITE algorithm’s ultimately goal is to reduce the overall time to solve each linear system.

We limited the comparison to coarse graphs ranging from 10 to 32 nodes to match the capabilities of our quantum simulator. We also used the LS-DYNA internal heuristic to compute the merit factors for graphs coarsened up to 50,000 nodes to get a sense of the performance of the system in the regime typically used for standard LS-DYNA production runs.

When the VarQITE algorithm converges, it produces a peaked distribution over the optimal/near-optimal GPP solutions. To understand the variation of the merit factor across these solutions, we investigated the merit factors for several of these near-optimal solutions in addition to the optimal solution.

The solutions found by VarQITE aim to minimize the total objective function, which is a combination of edge cut cost and nodal weight balance. We limit the evaluation of the merit factor to solutions that preserve the nodal weight balance within a 5% tolerance in order to maintain nodal weight balance as much as possible. The primary goal of this restriction is to allow for appropriate load balancing when LS-DYNA solves the actual linear system in parallel on multiple compute nodes. The weight balance is a heuristic hyperparameter, and more research is necessary to understand how it affects the total time to solution of the linear system.

Fig. 7 shows the merit factors obtained from a Level-1 nested dissection compared against the internal LS-DYNA classical heuristic. The VarQITE algorithm provides solutions with merit factors that are either equal or lower than LS-GPart solutions for graphs with 18 or more nodes. This is the case for both problem instances. Note that for graphs with a small number of nodes (≤ 16), LS-GPart produces solutions exceeding the 5% nodal weight balance threshold;

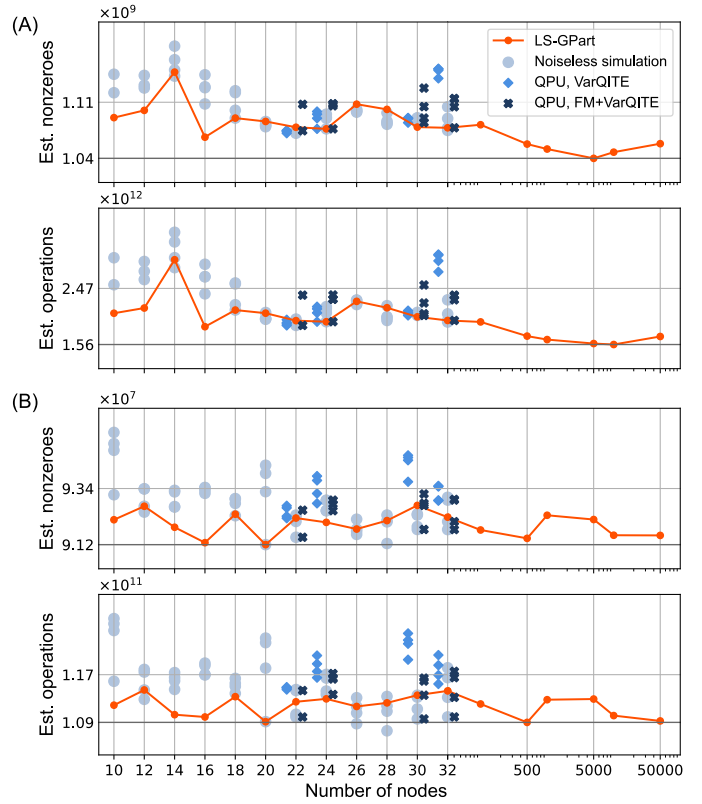


Fig. 7: Comparison of merit factors resulting from the VarQITE algorithm and the classical heuristic LS-GPart that is implemented in LS-DYNA. The two panels shown are (A) RoofCrush and (B) BloodPump, and each problem uses a Level 1 nested dissection. Each panel includes (top) the number of non-zeros (“fill-in”), and (bottom) the number of operations estimated from symbolic factorization by LS-DYNA. The VarQITE data is restricted to graph partitions that maintain a nodal weight balance within a 5% tolerance. The QPU data is from graphs with the same number of nodes as the corresponding simulation data, the plotting is offset for clarity. The plot also shows results from applying the modified FM algorithm to the QPU data. Shown on the horizontal axis are different numbers of nodes for the coarsened graph, corresponding to the number of qubits. Note that the largest varQITE experiments reported on have 32 nodes/qubits, however, the horizontal scale is extended logarithmically to much larger sizes of coarsening in order to capture the regime in which the classical LS-GPart heuristic operates. The 3 best solutions are plotted for each number of nodes/qubits in the coarsening, shown as the grey dots in the charts. As can be seen in the lower panel, for the BloodPump problem, solutions obtained by coarsening to 28 nodes lead to better merit factors when compared to LS-GPart (orange dots and lines) in terms of non-zeroes and in terms of factorization operations, even when compared to numbers of nodes that are as high as 50,000.

this is likely due to the limited options available. Because VarQITE solutions are restricted to those within the nodal

weight tolerance, the merit factors from VarQITE are higher than LS-GPart in these cases.

The decreasing trend in average merit factors as the number of nodes in the graph increases suggests that the VarQITE algorithm can generate solutions with even lower merit factors when applied to significantly larger graphs. Notably, for the BloodPump problem (Fig 7B) the VarQITE merit factors for the 26 and 28 nodes graph instances surpasses those from LS-GPart, even for graphs with 50,000 nodes. This demonstrates the potential for the VarQITE algorithm to provide benefit for specific problem types, even in the near term.

It is important to note that the optimal solution to the GPP problem does not always translate to the lowest merit factor. This is due to several factors, including the coarsening of the graph to a small number of nodes and the use of heuristics in the partitioning and matrix reordering processes. Even when the graph is coarsened to a standard production settings of 10,000–50,000 nodes, this holds true. The true advantage of using VarQITE in this context lies in its ability to produce a peaked distribution over multiple near-optimal solutions to the GPP. This allows for the evaluation of the merit factors for various solutions and the selection of the best one which, which can be significantly better than the single solution produced by LS-DYNA internal heuristic. As the quantum hardware advances and the qubit counts increase, the benefits of VarQITE for graph partitioning in terms of reducing overall FEA solution time will become increasingly apparent.

We extended the LS-DYNA nested dissection workflow to level 2. The optimal solution from level 1 was input into LS-DYNA to obtain the level 2 coarse graphs. VarQITE was then used to compute graph partitions to the level 2 coarse graphs, and the merit factors were computed. Further details are available in the Supplementary Information (SI) VI-A.

C. Measuring total wall clock time for the linear solver

In addition to the merit figure computations obtained in Section IV-B, we conducted experiments to investigate how the partitions produced by our VarQITE-powered GPP solver impact the wall clock time (WCT) required by LS-DYNA to execute a linear system solve. For these simulations we used the RoofCrush and BloodPump problems from the previous section, as well as the VibrationAnalysis problem from Table I. For the BloodPump problem, we refined the previously used mesh to increase the number of vertices to 2.6 million and the number of edges to 40 million.

Figure 8 shows the comparison of the total WCT required for a linear system solve when using LS-DYNA’s internal partitioner and when using our VarQITE-powered GPP solver. The figures explore how the total WCT scales as a function of the number of nodes in the coarsened graph. The plot compares the resulting WCTs when running LS-DYNA’s internal vs. our external partitioner, normalized with respect to the WCT required by the reference code, which is LS-DYNA configured with its production settings (graphs coarsened to 10,000 nodes). In order to obtain realistic results, we distributed these computations across 8, 16, or 24 MPI

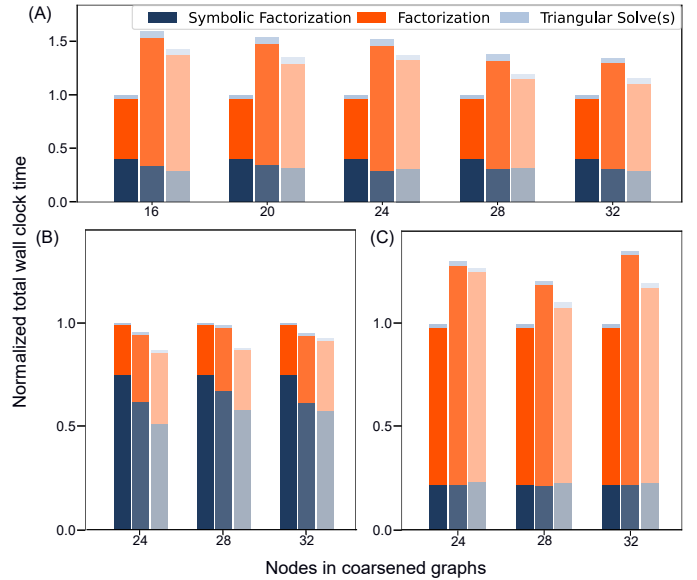


Fig. 8: Total wall clock time (WCT) comparison for linear system solve of the (A) RoofCrush problem on 8 MPI ranks, (B) BloodPump problem on 24 MPI ranks and (C) VibrationAnalysis problem on 16 MPI ranks. All simulations were done on a 4 Intel Xeon Gold 6242 CPUs, 64 cores in total; and 1.5TB memory. In each group, the leftmost bar represents total WCT when coarsening the graph to 10,000 nodes (production setting in LS-DYNA/LS-GPart). The middle and right bars compare WCT when coarsening the graph to different numbers of nodes shown on the horizontal axis, and using the internal (LS-DYNA) vs. the external (varQITE-based) partitioner, i.e., the bars on the right show the quantum-enhanced performance. Note that the external partitioner leads to shorter WCT for all experiments shown in this figure. Further, there is a trend in case of RoofCrush in that the wall clock times seem to decrease with increasing number of qubits. Finally, in case of BloodPump, the WCT of the solver resulting from the varQITE partitioner is lower than the WCT of the production solver. The differences of the left to the right bar in panel (B) are, reading from left to right, -11.93% , -11.51% , and -9.80% . This means that the quantum solution improved over the industry-grade heuristic by close to 12%;

ranks, much like a typical LS-DYNA user. Every experiment was conducted on the same machine, built with 4 Intel Xeon Gold 6242 CPUs, 16 cores each, and 1.5TB of memory. As explained in Section III-C, our partitioner yields a distribution over high-quality solutions to the underlying GPP. Figure 8 displays the results of the partition yielding the lowest WCT amongst the 10 lowest energy partitions in the partitioner’s optimized distribution. For these experiments, we refined the mesh of the BloodPump problem by making it 100x more dense so the factorization time was meaningful enough to measure improvements.

The figures provide concrete evidence that our VarQITE-

powered partitioner improves upon LS-DYNA’s internal graph partitioner in most cases, when used on the same coarsened graph. This shows that the VarQITE algorithm is able to provide partitions that improve the WCT across different FEA models displaying the applicability of the algorithm to a spectrum of different problem types. Figure 8a illustrates a decreasing trend in WCT for the RoofCrush problem as we increase the number of nodes in the coarsened graph. The same trend can be noticed in Figure 8c for the VibrationAnalysis problem (although there is a little more noise in this case). The decreasing trend provides confidence that the VarQITE algorithm could be scaled to much larger graph sizes and would continue to improve the WCT, matching and even improving upon the production settings (graphs coarsened to 10,000 nodes) in the near future. In addition, Figure 8b suggests there are some problem geometries where we may find comparable WCT when coarsening to a few dozen nodes as we do when coarsening to the production-level of 10,000 nodes. This result is quite encouraging as a stepping-stone towards quantum utility, as it suggests there are certain problem types where we may find early advantage when using a VarQITE-powered partitioner over leading existing classical methods.

D. Hardware experiments

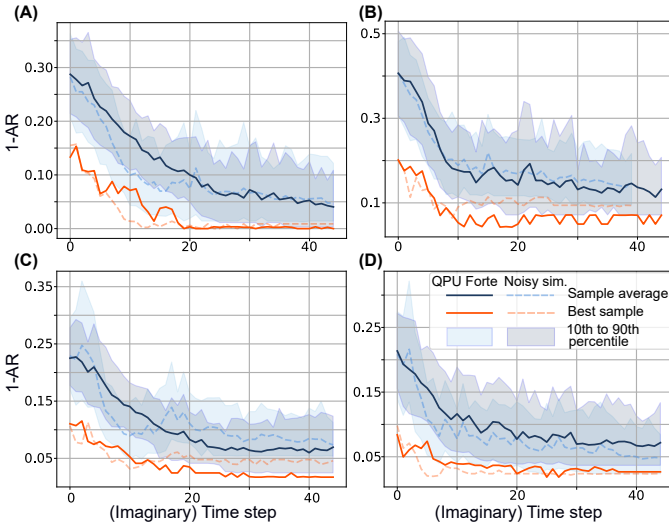


Fig. 9: Plots of convergence of VarQITE on IonQ QPU Forte, (A) RoofCrush 30 nodes, (B) RoofCrush 32 nodes, (C) BloodPump 30 nodes, (D) BloodPump 32 nodes. The y axis shows the value of 1-AR where AR is the approximation ratio of the solution. The solid blue line and solid purple line correspond to the average and best value sampled on IonQ Forte. The dashed green line and dashed purple line correspond to the average and best value sampled using the IonQ noisy simulator. The shaded blue and green regions correspond to the values of solutions between the 10th and 90th percentile in the sampled distribution.

A few select graph instances from the RoofCrush and BloodPump problems were executed on IonQ quantum processing units (QPUs) Aria and Forte. The IonQ Aria QPU uses

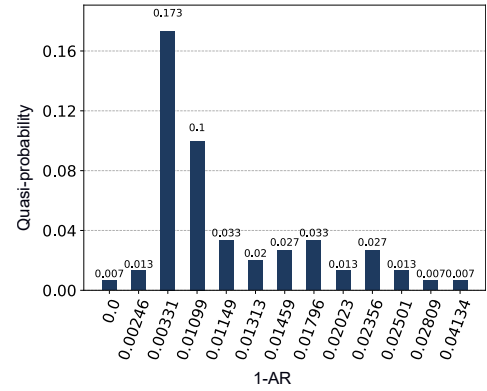


Fig. 10: Probability histogram of a few unique solutions with the lowest objective function values from RoofCrush GPP problem coarsened to 30 nodes. The x-axis shows solutions with increasing values of 1 - Approximation Ratio. The first bar from the left with the 1-AR value of 0.0 is the optimal solution to the GPP problem.

up to 25 addressable Ytterbium (Yb) ions linearly arranged in an ion trap, while the IonQ Forte QPU has 36 addressable Ytterbium (Yb) ions. Qubit states are implemented by utilizing two states in the ground hyperfine manifold of the Yb ions. Manipulating the qubits in the Aria and Forte QPUs is done using mode-locked 355nm laser pulses, which drive Raman transitions between the qubit states. By configuring these pulses, arbitrary single-qubit gates and Mølmer-Sørensen type two-qubit gates [16] can both be realized. As of this publication, the Aria QPU has demonstrated performance at the level of 25 algorithmic qubits and the Forte QPU has demonstrated performance at the level of 36 algorithmic qubits [17]–[20]. In order to mitigate the effect of systematic errors on the Aria/Forte QPU, error mitigation via symmetrization was used [21]. After executing multiple circuit variants with distinct qubit to ion mappings, the measurement statistics was aggregated using component-wise averaging.

Graph partitioning problems from both the RoofCrush and BloodPump problem instances with 22 and 24 nodes were executed on IonQ Aria and graph partitioning problems with 30 and 32 nodes were executed on IonQ Forte. The graph problems were chosen to demonstrate the performance of the VarQITE algorithm and the IonQ QPUs as a function of problem size as well as the capability to handle different types of graphs for a given problem size. To execute VarQITE algorithm on the QPU, the HeavyNeighborsAnsatz described in III-B was used with 60 parametrized R_{ZY} gates for the RoofCrush problem instance and 82 parametrized R_{ZY} gates for the BloodPump problem instance. The number of gates in the ansatz was chosen taking into account the total QPU execution time for the algorithm and the fact that the ansatz does not necessarily require gates across all pairs of qubits to solve these graph problems. The number of two-qubit gates selected in the truncated ansatz balances the ansatz expressibility, the deleterious effects of QPU noise as more

gates are added, and the total execution time on the QPU.

The hardware execution began with all variational parameters in the ansatz initialized to zero, with the initial state $|+\rangle^{\otimes}$ obtained from Hadamard gates applied to $|0\rangle^{\otimes}$ state. All measurements of the quantum circuits were performed in the computational basis with 128 shots per circuit evaluation and measurement. The hybrid quantum optimization algorithm was executed entirely on the IonQ QPU hardware from initialization until convergence. The evolution of the average error (defined as 1-AR) as a function of the iterations of the VarQITE algorithm is shown in Fig 9 for graphs of sizes 30 and 32 from both the RoofCrush and BloodPump problem instances executed on IonQ Forte. The average error decreases steadily as the higher energy eigenstates of the hamiltonian are projected out and the final distribution peaks on/near the optimal solution. The algorithm converges fairly rapidly to the optimal distribution. This demonstrates the robustness of the VarQITE algorithm to both shot noise (128 shots per circuit measurement) and QPU noise along with its excellent performance on different types of graphs with differently weighted edges and connectivity. In all cases, the algorithm is able to attain an average error rate of $< 20\%$ and a best sample error rate of $< 5\%$. Figure 10 shows the sampled distribution from the last iteration of the VarQITE algorithm for RoofCrush GPP problem with 30 nodes executed on IonQ Forte. The first bar from the left represents the optimal solution to the problem with a 1-AR value of 0.0. Various other near-optimal solutions have also been sampled showing that the VarQITE algorithm has succeeded in converging to a distribution peaked over the optimal and near-optimal solutions. The plots of convergence of VarQITE runs on IonQ Aria and the probability histogram plots for all problem instances executed on IonQ QPUs are provided in the Supplementary Information Section VI-A.

The merit factors computed from the solutions obtained from quantum hardware are shown in Figure 7. The hardware merit factors are close to the simulation merit factors showing the high quality of solutions found on IonQ hardware and the robustness of the VarQITE algorithm. For the largest problem sizes of 30 and 32 qubits, the hardware merit factors are higher than the simulation merit factors due to QPU noise and shot noise. With further improvements in the fidelity of quantum hardware, solutions with lower merit factors can be found. In order to improve the merit factors of the solutions, the modified FM algorithm was used to refine the solutions by taking the solutions obtained from the hardware runs as input. These are shown in Figure 7 as “FM+VarQITE”. The merit factors from these solutions match the best simulation data and outperform the LS-DYNA classical heuristic for many problem instances, e.g., for the BloodPump problem. The modified FM algorithm can thus be used as a means of error mitigation on noisy QPU results to recover high quality solutions with low merit factors. This demonstrates the high performance and robustness of the combined “VarQITE+modified FM” approach making the use of near term quantum hardware to deliver tangible enhancements to certain large scale industrial problems a definite possibility in the near future.

V. CONCLUSIONS AND OUTLOOK

We developed and demonstrated a pipeline for the integration of the VarQITE quantum algorithm into an industrial workflow for solving large scale problems in Finite Element Analysis. We have shown that the VarQITE algorithm may be used to solve the graph partitioning problem arising in the solution of large sparse linear systems in various domains from mechanical engineering to computational fluid dynamics. Our results show that the VarQITE algorithm is able to provide partitions that improve the WCT across different FEA models displaying the applicability of the algorithm to different problem types. These results provide confidence that the VarQITE algorithm could be scaled to much larger graph sizes and would continue to improve the WCT, matching and even improving upon the production settings (graphs coarsened to 10,000 nodes) in the near future.

We have also demonstrated full hybrid on-QPU optimization of the graph partitioning problem for graphs of varying types, connectivity and sizes on IonQ Aria and IonQ Forte QPUs. Our results have shown that the VarQITE algorithm is capable of finding optimal solutions to the GPP for graphs coarsened up to 32 nodes with convergence to high optimal solution probability. The high quality of results obtained for the different types of problems studied suggests the robustness of the algorithm in solving generic instances of the graph partitioning problem arising in industrially relevant large scale FEA problems. The high quality results also demonstrate the robustness of the quantum algorithm against shot noise and QPU noise even at 32 qubits on quantum hardware.

Our results show that there are some problem geometries where we may find improvements to WCT when coarsening to a few dozen nodes as we do when coarsening to the industrial-level of 10,000 nodes suggesting there are certain problem types where we may find early advantage when using a VarQITE-powered partitioner over leading existing classical methods. Since QPU executions can often take much longer than classical CPUs/GPUs (at least in the near term), it is important to find problems where the QPU call is executed once or at most a few times in the classical workflow. Such problems arise in problems such as vibrational analysis, finding failure modes etc. where the problem requires the determination of the lowest eigenmodes of the matrix which can be computationally expensive. A superior reordering of the matrix provided by a better solution from VarQITE can have a much larger impact in the total WCT for such problems as compared to problems in dynamics. These and other such problems should become the focus of investigation of quantum commercial utility in the near term as quantum hardware continues to scale and improve. The low circuit depth of our ansatz, the minimal resource requirements of the VarQITE algorithm, superior empirical performance, and scalability of our approach make it a promising candidate for solving these and other interesting industrial scale problems in the future.

REFERENCES

- [1] M. Yannakakis, "Computing the minimum fill-in is np-complete," *SIAM Journal on Algebraic Discrete Methods*, vol. 2, no. 1, pp. 77–79, 1981.
- [2] A. George, "Nested dissection of a regular finite element mesh," *SIAM journal on numerical analysis*, vol. 10, no. 2, pp. 345–363, 1973.
- [3] "Metis: a software package for partitioning unstructured graphs, partitioning meshes, and computing fill-reducing orderings of sparse matrices," technical report, Department of Computer Science, University of Minnesota, 1998.
- [4] K. Andreev and H. Racke, "Balanced graph partitioning," *Theory of Computing Systems*, vol. 39, no. 6, p. 929–939, Oct 2006.
- [5] T. D. Morris and P. C. Lotshaw, "Performant near-term quantum combinatorial optimization," *arXiv preprint arXiv:2404.16135*, 2024.
- [6] "Ansys Is-dyna," <https://www.ansys.com/products/structures/ansys-is-dyna>.
- [7] X. Yuan, S. Endo, Q. Zhao, Y. Li, and S. C. Benjamin, "Theory of variational quantum simulation," *Quantum*, vol. 3, no. 191, p. 191, Oct. 2019. [Online]. Available: <https://quantum-journal.org/papers/q-2019-10-07-191/pdf/>
- [8] S. McArdle, T. Jones, S. Endo, Y. Li, S. C. Benjamin, and X. Yuan, "Variational ansatz-based quantum simulation of imaginary time evolution," *Npj Quantum Inf.*, vol. 5, no. 1, pp. 1–6, Sep. 2019. [Online]. Available: <https://www.nature.com/articles/s41534-019-0187-2>
- [9] T. D. Morris, A. Kaushik, M. Roetteler, and P. C. Lotshaw, "Performant near-term quantum combinatorial optimization," *arXiv [quant-ph]*, 24 Apr. 2024. [Online]. Available: <http://arxiv.org/abs/2404.16135>
- [10] K. Mitarai, M. Negoro, M. Kitagawa, and K. Fujii, "Quantum circuit learning," *Phys. Rev. A*, vol. 98, no. 3, p. 032309, Sep. 2018. [Online]. Available: <http://link.aps.org/pdf/10.1103/PhysRevA.98.032309>
- [11] M. Schuld, V. Bergholm, C. Gogolin, J. Izaac, and N. Killoran, "Evaluating analytic gradients on quantum hardware," *Phys. Rev. A*, vol. 99, no. 3, p. 032331, Mar. 2019. [Online]. Available: <http://link.aps.org/pdf/10.1103/PhysRevA.99.032331>
- [12] B. W. Kernighan and S. Lin, "An efficient heuristic procedure for partitioning graphs," *The Bell system technical journal*, vol. 49, no. 2, pp. 291–307, 1970.
- [13] C. M. Fiduccia and R. M. Mattheyses, "A linear-time heuristic for improving network partitions," in *Papers on Twenty-five years of electronic design automation*, 1988, pp. 241–247.
- [14] A. Gatti, Z. Hu, T. Smidt, E. G. Ng, and P. Ghysels, "Graph partitioning and sparse matrix ordering using reinforcement learning and graph neural networks," *Journal of Machine Learning Research*, vol. 23, no. 303, pp. 1–28, 2022.
- [15] D. Kucar, S. Areibi, and A. Vannelli, "Hypergraph partitioning techniques," *Dynamics of Continuous Discrete and Impulsive Systems Series A*, vol. 11, pp. 339–368, 2004.
- [16] A. Sørensen and K. Mølmer, "Quantum computation with ions in thermal motion," *Physical review letters*, vol. 82, no. 9, p. 1971, 1999. [Online]. Available: <https://journals.aps.org/prl/abstract/10.1103/PhysRevLett.82.1971>
- [17] "Ionq, algorithmic qubits: A better single number metric," <https://ionq.com/resources/algorithmic-qubits-a-better-single-number-metric>.
- [18] "Ionq aria," <https://ionq.com/quantum-systems/aria>.
- [19] "Ionq forte," <https://ionq.com/quantum-systems/forte>.
- [20] T. Lubinski, S. Johri, P. Varosy, J. Coleman, L. Zhao, J. Necaie, C. H. Baldwin, K. Mayer, and T. Proctor, "Application-oriented performance benchmarks for quantum computing," *IEEE Transactions on Quantum Engineering*, 2023. [Online]. Available: <https://ieeexplore.ieee.org/abstract/document/10061574>
- [21] A. Maksymov, J. Nguyen, Y. Nam, and I. Markov, "Enhancing quantum computer performance via symmetrization," *arXiv preprint arXiv:2301.07233*, 2023. [Online]. Available: <https://arxiv.org/abs/2301.07233>

VI. SUPPLEMENTARY INFORMATION

A. Statistics of VarQITE refinement with the modified FM algorithm

Here we show the results from applying the modified FM algorithm to the VarQITE results from IonQ Forte. Fig 11 shows a comparison of the histograms from the raw VarQITE results and after refining using the modified FM algorithm.

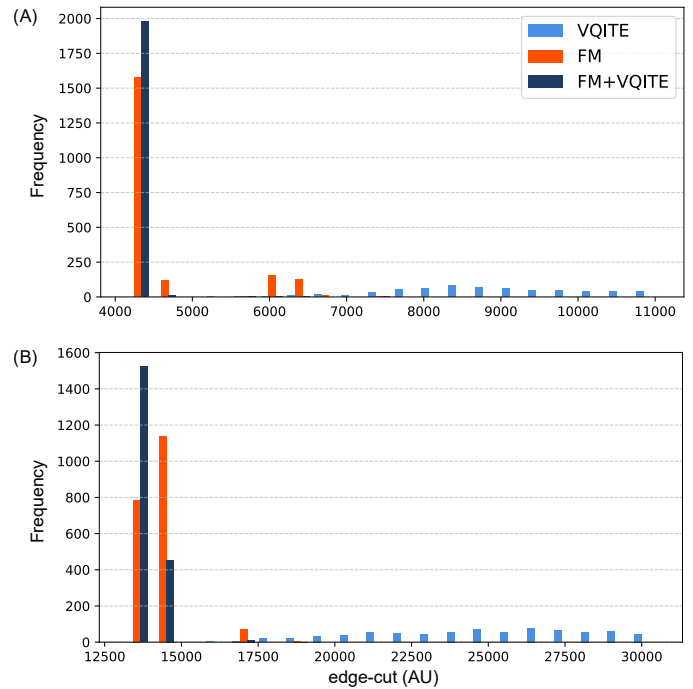


Fig. 11: Histograms of partition distributions binned by evaluated edge-cut cost for two benchmark problems: (A) RoofCrush and (B) BloodPump. The partitions are obtained using three different methods: FM (Fiduccia-Mattheyses) with random (equal-cardinality) initialization, VarQITE, and FM initialized with VarQITE partitions (FM+VarQITE). Each method generates 2,000 partitions, with VarQITE sampling 2,000 times, FM using 2,000 random initializations, and FM+VarQITE refining the 2,000 partitions from VarQITE. Partitions with $> 5\%$ imbalance are filtered out per problem constraints. A method is considered superior if it yields more partitions in total and more partitions toward the left, indicating lower edge-cut costs.

The results also include using the modified FM algorithm alone from a random distribution of solutions of equal cardinality. The figure shows that a superior set of solutions can be found from the "VarQITE+FM" method as compared to using VarQITE or FM alone.

B. Comparison of merit factors between VarQITE noiseless simulations and LS-DYNA - Level 2 nested dissection

Here we show the merit factors obtained from noiseless simulations of the VarQITE algorithm on Level 2 nested dissection graphs for the RoofCrush and BloodPump problems. Figure 12 shows the comparison of merit factors from VarQITE and LS-GPart. The figure shows encouraging results as there are simulation points that show lower merit factors than LS-GPart, especially for the BloodPump problem. There is an additional nuance here since the results depend on the specific solution chosen for the Level 1 graph partitioning. There are many cases where LS-GPart chooses a Level 1 solution that is outside the 5% nodal weight balance which can result in

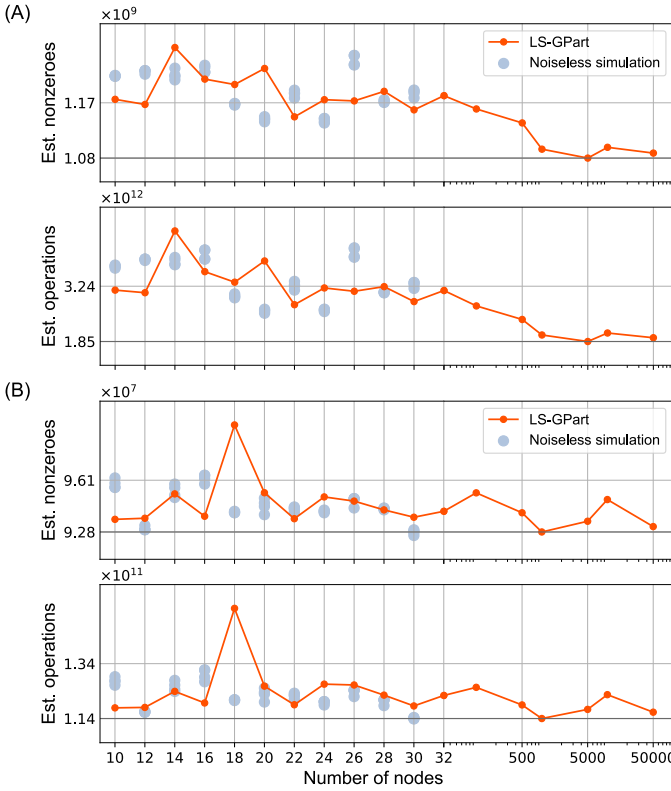


Fig. 12: Plot of merit factors obtained from the VarQITE algorithm executed on (A) the RoofCrush problem and (B) the BloodPump problem at Level 2 nested dissection compared with the classical heuristic in LS-DYNA (LS-GPart): (top) The number of non-zeros (“fill-in”), (bottom) The number of operations estimated from symbolic factorization by LS-DYNA. The VarQITE data is only from graph partitions which maintain a nodal weight balance within a 5% tolerance. The QPU data is from graphs with the same number of nodes as the corresponding simulation data, just offset from the simulation points for clarity. The plot also shows the results of applying the modified FM algorithm to the QPU data. This plot should be compared to Fig. 7 in that it shows similar behavior for the BloodPump case, where solutions coarsened to 30 nodes/qubits are competitive with LS-GPart at up to 10,000 nodes.

a lower merit factor for Level 2. But the VarQITE solutions always respect the 5% nodal weight balance. This makes the data shown in Fig 12 a little more noisy for the RoofCrush problem.

C. Additional data: measuring wall clock time for linear solve

Here we show additional wall clock time experiments from the RoofCrush, BloodPump and VibrationalAnalysis problems. Figures 13, 14 and 15 show the results from running on different numbers of MPI ranks. The results still show a largely decreasing trend of WCT from VarQITE solutions with increasing number of nodes of the coarsened graph. The VarQITE solutions also show an improvement over LS-GPart

in most cases, but not all. The cases where VarQITE does not show an improvement over LS-GPart need further investigation with likely causes ranging from incomplete convergence of VarQITE to near optimal solutions to control over the compute environment while computing WCT.

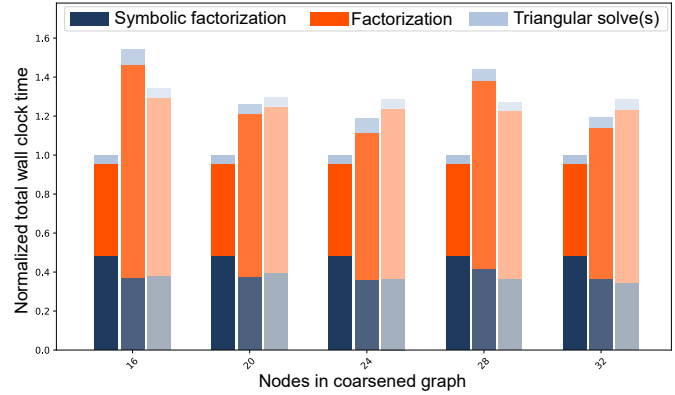


Fig. 13: Total WCT comparison for linear system solve of the RoofCrush problem on 16 MPI ranks. The leftmost bar represents total WCT when coarsening the graph to 10,000 nodes (production setting). The middle and right bars compare WCT when coarsening the graph to different numbers of nodes shown on the x-axis, and using the internal vs. the external partitioner

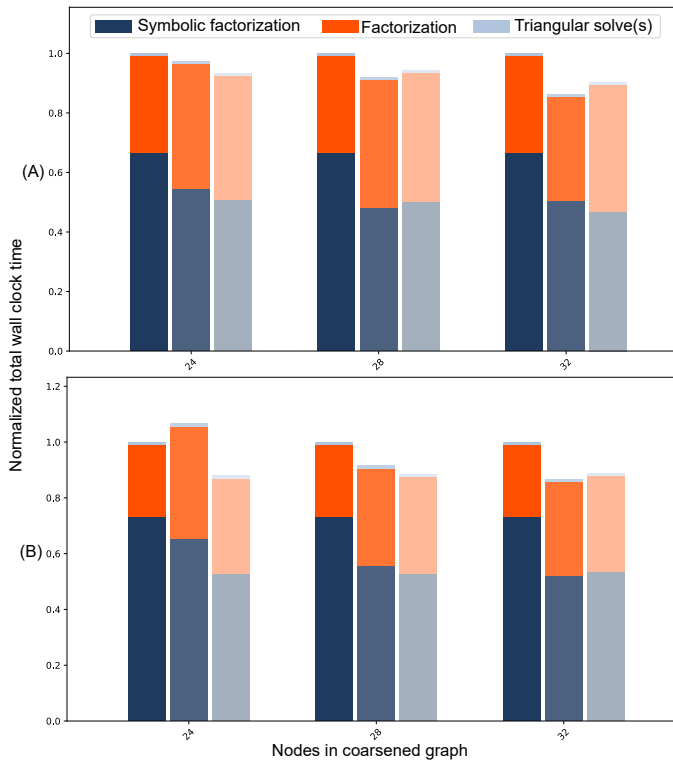


Fig. 14: Total WCT comparison for linear system solve of the BloodPump problem on A) 8 MPI ranks and B) 16 MPI ranks. In each group, the leftmost bar represents total WCT when coarsening the graph to 10,000 nodes (production setting). The middle and right bars compare WCT when coarsening the graph to different numbers of nodes shown on the x-axis, and using the internal vs. the external partitioner

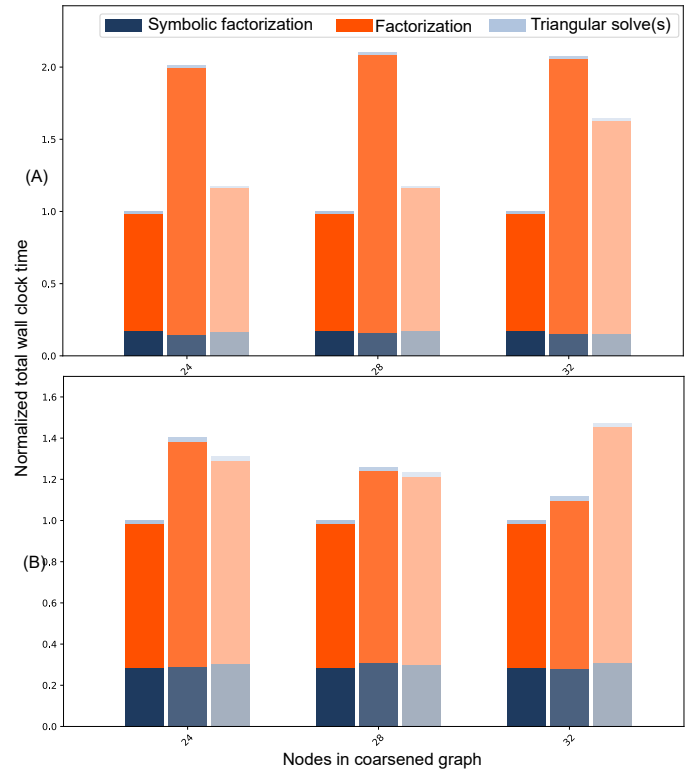


Fig. 15: Total WCT comparison for linear system solve of the VibrationAnalysis problem on A) 8 MPI ranks and B) 24 MPI ranks. In each group, the leftmost bar represents total WCT when coarsening the graph to 10,000 nodes (production setting). The middle and right bars compare WCT when coarsening the graph to different numbers of nodes shown on the x-axis, and using the internal vs. the external partitioner